Biochem. J. (2013) **449**, 39–49 (Printed in Great Britain) doi:10.1042/BJ20121034

Activation of IP_3 receptors requires an endogenous 1-8-14 calmodulin-binding motif

Yi SUN[1,2], Ana M. ROSSI[1], Taufiq RAHMAN and Colin W. TAYLOR[3]

Department of Pharmacology, University of Cambridge, Cambridge CB2 1PD, U.K.

Binding of IP_3 (inositol 1,4,5-trisphosphate) to the IP_3-binding core (residues 224–604) of IP_3Rs (IP_3 receptors) initiates opening of these ubiquitous intracellular Ca^{2+} channels. The mechanisms are unresolved, but require conformational changes to pass through the suppressor domain (residues 1–223). A calmodulin-binding peptide derived from myosin light chain kinase uncouples these events. We identified a similar conserved 1-8-14 calmodulin-binding motif within the suppressor domain of IP_3R1 and, using peptides and mutagenesis, we demonstrate that it is essential for IP_3R activation, whether assessed by IP_3-evoked Ca^{2+} release or patch-clamp recoding of nuclear IP_3R. Mimetic peptides specifically inhibit activation of IP_3R by uncoupling the IP_3-binding core from the suppressor domain. Mutations of key hydrophobic residues within the endogenous 1-8-14 motif mimic the peptides. Our results show that an endogenous 1-8-14 motif mediates conformational changes that are essential for IP_3R activation. The inhibitory effects of calmodulin and related proteins may result from disruption of this essential interaction.

Key words: 1-8-14 motif, calcium signalling, calmodulin, inositol 1,4,5-trisphosphate receptor, myosin light chain kinase (MLCK).

INTRODUCTION

Ca^{2+} channels allow most electrical and many chemical signals to be transduced into the changes in cytosolic Ca^{2+} concentration that regulate almost every aspect of cellular activity [1]. Most Ca^{2+} channels are also regulated by Ca^{2+}, either directly or via CaM (calmodulin) [2]. This provides feedback regulation of Ca^{2+} signalling and it allows Ca^{2+} channels to evoke regenerative Ca^{2+} signals [3]. The latter are important because they underpin the versatility of Ca^{2+} as an intracellular messenger, permitting it to function either locally or globally [1].

Two major families of intracellular Ca^{2+} channels, IP_3Rs [IP_3 (inositol 1,4,5-trisphosphate) receptors] and RyRs (ryanodine receptors), share many structural [4,5] and functional [5–7] properties. Most notably, all IP_3Rs and RyRs are stimulated by low concentrations of cytosolic Ca^{2+} and inhibited by higher concentrations. Ca^{2+}-binding sites within the RyR itself can mediate this biphasic Ca^{2+} regulation [7], but, for IP_3Rs, it remains unclear whether additional Ca^{2+}-binding proteins are required [6]. None of the many Ca^{2+}-binding sites in RyRs [8] or IP_3Rs [9] has been unambiguously associated with Ca^{2+} regulation of channel gating [10,11], although mutation of a single equivalent residue in RyRs or IP_3Rs (Glu^{2100} in IP_3R1) modulates their Ca^{2+}-sensitivity [11]. Both families of intracellular Ca^{2+} channels are also regulated by CaM, a ubiquitously expressed and highly conserved Ca^{2+}-binding protein [12]. Related proteins with EF-hand Ca^{2+}-binding structures, such as S100A and CaBP1 (Ca^{2+}-binding protein 1), also regulate RyRs and IP_3Rs, but the physiological significance of these interactions between intracellular Ca^{2+} channels and CaM or related proteins is unresolved [13,14]. Despite some conflicting evidence [15], CaM seems not to be essential for Ca^{2+} regulation of RyRs or IP_3Rs [16–18], but it does regulate both channels and it modulates their responses to Ca^{2+} [19–21].

All IP_3Rs are inhibited by Ca^{2+}–CaM [22], but neither of the two CaM-binding sites within IP_3R1, nor a third that is created by alternative splicing [23], clearly mediates this inhibition of IP_3-evoked Ca^{2+} release. The central site [24] (Figure 1A) mediates neither Ca^{2+} nor CaM regulation of IP_3R activity [16,17] and it is absent from IP_3R3. The functional role of the split N-terminal site (Figure 1A), one component of which may also bind CaBP1 [25], is also unclear. It has been proposed to bind CaM and thereby to inhibit IP_3R activity, but only when Ca^{2+} has bound elsewhere [26]. The evidence that CaM inhibits IP_3R only in the presence of Ca^{2+}, without CaM itself providing the Ca^{2+}-sensor, is persuasive [26], but there is no compelling evidence to link this to the N-terminal CaM-binding site [27].

The links between CaM binding and function are better understood for RyRs, although the effects differ between RyR subtypes [7]. A single site on each RyR1 subunit (residues 3614–3643 in rabbit RyR1), which is conserved in all RyRs, binds the C-terminal lobe of both apo-CaM and Ca^{2+}–CaM and appears to mediate the functional effects of CaM [20,28,29]. As this tethered CaM binds Ca^{2+}, it migrates towards the NT (N-terminus) of the binding site and the CaM switches from activating RyR1 to inhibiting it [19]. The CaM-binding site of RyR1 also engages other CaM-like domains, notably the C-terminus of the L-type Ca^{2+} channel which inhibits RyR1 activity [30], and perhaps an EF-hand-like structure within the C-terminal region of RyR1 which binds Ca^{2+} and modulates Ca^{2+} regulation of RyR [31]. These observations suggest that the CaM-binding domain of RyR also mediates important inter- and intra-molecular interactions, and that the complex effects of CaM and related proteins may, at least in part, result from disrupting these interactions [29,31,32].

Abbreviations used: BCR, B-cell receptor; CaBP1, Ca^{2+}-binding protein 1; CaM, calmodulin; CLM, cytosol-like medium; IP_3, inositol 1,4,5-trisphosphate; IBC, IP_3-binding core; IP_3R, IP_3 receptor; MLCK, myosin light chain kinase; NT, N-terminus; RyR, ryanodine receptor; SD, suppressor domain.

[1] These authors contributed equally to this work.

[2] Present address: Wellcome Trust Sanger Institute, Wellcome Trust Genome Campus, Hinxton, Cambridge CB10 1SA, U.K.

[3] To whom correspondence should be addressed (email cwt1000@cam.ac.uk).

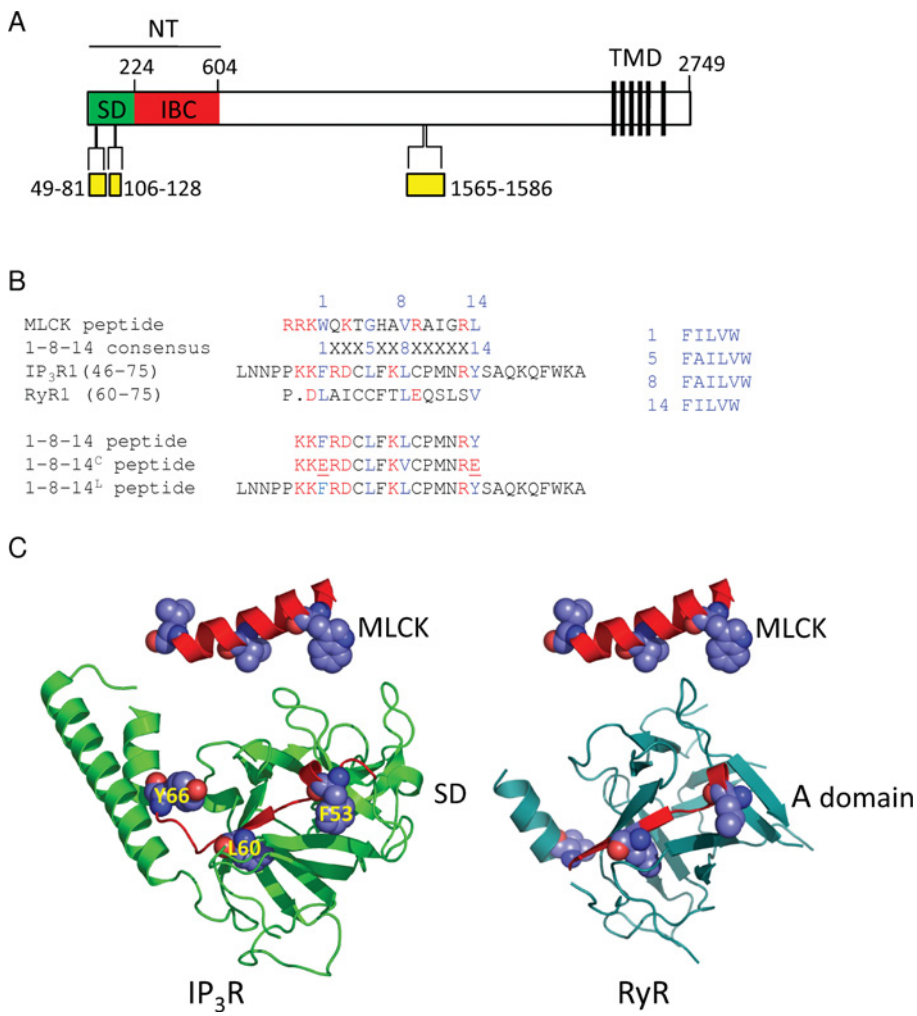

Figure 1 A putative 1-8-14 motif within the SD of the IP_3R

(**A**) Key features of a rat IP_3R showing the NT, with its component parts (SD and IBC), the six C-terminal transmembrane domains (TMD) that form the pore and the CaM-binding domains (yellow). Residue numbers are shown. (**B**) Comparison of 1-8-14 motifs showing the conserved hydrophobic residues of the consensus sequence in blue. Charged residues within the 1-8-14 motif are highlighted in red because the consensus motif has a net charge of $+3$ to $+6$. The lower panel shows the peptides used with mutated residues underlined. (**C**) Structure of the SD of IP_3R1 (PDB code 1XZZ) and the equivalent region (A domain) of RyR1 (PDB code 3HSM) with the pseudo-1-8-14 motif highlighted and compared with MLCK in the structure it adopts when bound to Ca^{2+}–CaM (PDB code 1QTX).

For IP_3Rs, IP_3 binding to the IBC (IP_3-binding core) (residues 224–604) (Figure 1A) initiates the conformational changes that lead to opening of a pore formed by the C-terminal transmembrane domains of each of the four IP_3R subunits [5,33]. These conformational changes pass via the N-terminal SD (suppressor domain) (residues 1–223), which is essential for IP_3R activation. Indeed, the major conformational changes associated with IP_3R activation appear to occur within the NT (residues 1–604) [5,33]. Although both IP_3 and Ca^{2+} are required for IP_3R activation [6,34], it is not yet clear how the conformational changes initiated by IP_3 lead to Ca^{2+} binding and then to gating of the pore. It is therefore intriguing that a CaM-binding peptide derived from MLCK (myosin light chain kinase), which comprises a 1-8-14 CaM-binding sequence [35], reversibly inhibits IP_3-evoked Ca^{2+} release [36] via all three vertebrate IP_3R subtypes. Furthermore, MLCK peptide is more potent in the presence of Ca^{2+} [35]. This inhibition is entirely independent of CaM and involves interaction of MLCK peptide with the NT in a manner that requires the SD [35]. We speculate, by analogy with RyRs, that inhibition of IP_3Rs by MLCK peptide might result from disruption of an interaction between endogenous CaM-like and CaM-binding domains within IP_3Rs, and that, for IP_3Rs, this interaction is essential for activation. In the present study, we explored this hypothesis further.

EXPERIMENTAL

Materials

Cell culture materials were from Gibco, except for fetal bovine serum (Sigma). CaM purified from bovine brain was from Calbiochem. [^{3}H]IP_3 (18 Ci/mmol) was from PerkinElmer. IP_3 was from Alexis Biochemicals. Peptides were synthesized and purified by Sigma or New England Peptide, and each was shown to be >90 % pure by HPLC. The peptide sequences are listed in Supplementary Table S1 (at http://www.biochemj.org/bj/449/bj4490039add.htm).

Site-directed mutagenesis

The NT (residues 1–604) and IBC (residues 224–604) of rat IP_3R1 were amplified by PCR from the full-length receptor clone lacking the SI splice region (GenBank® accession number GQ233032.1) as described previously [33]. The fragments were ligated into pTrcHis A (Invitrogen) to allow expression of N-terminally His_6-tagged proteins. Mutagenesis of the 1-8-14 motif within the NT used the QuikChange® II XL site-directed mutagenesis kit (Stratagene) for single mutants (F53E, L60E, Y66E and K52E) and the QuikChange® multi-site-directed mutagenesis kit for the double mutant (F53E and Y66E). The primers used are listed in Supplementary Table S2 (at http://www.biochemj.org/bj/449/bj4490039add.htm). The same primers and conditions were used for mutagenesis of full-length IP_3R using IP_3R1 in the pENTR 1A vector. Full-length constructs were subcloned into pcDNA3.2/V5-DEST for expression in DT40 cells. The complete sequence of every mutant construct was verified by sequencing.

Culture and stable transfection of DT40 cells

DT40 cells in which the genes for all three IP_3R subtypes had been disrupted (DT40-KO) [37] and DT40 cells stably expressing rat IP_3R1 (DT40-IP_3R1) were grown in RPMI 1640 medium supplemented with 10 % (v/v) fetal bovine serum, 1 % (v/v) heat-inactivated chicken serum, 2 mM L-glutamine and 50 μM 2-mercaptoethanol. Cells were grown in suspension in 175 cm^2 flasks at 37 °C in an atmosphere of 5 % CO_2. They were used or passaged when they reached a density of $\sim 2\times10^6$ cells/ml. To generate stable cell lines expressing mutant IP_3R, the mutant construct in pcDNA3.2/V5-DEST was linearized, and DT40 cells were transfected by nucleofection (Amaxa, protocol B-23). Cell lines were selected with G-418 (2 mg/ml) and screened initially by Western blotting using a peptide antiserum to IP_3R1 [38] as described previously [33], and then using the functional assay described below.

Ca^{2+} release from the intracellular stores of permeabilized cells

The free Ca^{2+} concentration of the intracellular stores of permeabilized cells was measured using a low-affinity Ca^{2+} indicator trapped within the endoplasmic reticulum as reported previously [39]. Briefly, DT40 cells (4×10^7 cells/ml) were suspended in HBS (Hepes-buffered saline: 135 mM NaCl, 5.9 mM KCl, 11.6 mM Hepes, 1.5 mM $CaCl_2$, 11.5 mM glucose and 1.2 mM $MgCl_2$, pH 7.3) containing 1 mg/ml BSA, 0.4 mg/ml Pluronic F127 and 20 μM mag-fluo-4/AM (Invitrogen). After 1 h at 20 °C in the dark with gentle shaking, cells were centrifuged at 650 ***g*** for 2 min and resuspended to 10^7 cells/ml in Ca^{2+}-free CLM (cytosol-like medium) (20 mM NaCl, 140 mM KCl, 1 mM EGTA, 20 mM Pipes and 2 mM $MgCl_2$, pH 7.0) containing 20 μg/ml saponin. After incubation at 37 °C with gentle shaking for 4 min, permeabilized cells were centrifuged at 650 ***g*** for 2 min and resuspended in Mg^{2+}-free CLM, supplemented with $CaCl_2$ to give a final free Ca^{2+} concentration of 220 nM. The free Ca^{2+} concentration of CLM was calculated using the MaxChelator program (http://maxchelator.stanford.edu) and then measured using fluo-3 or fura-2. Cells were then washed, resuspended in Mg^{2+}-free CLM containing 10 μM FCCP (carbonyl cyanide *p*-trifluoromethoxyphenylhydrazone) to inhibit mitochondria, and distributed into a 96-well plate (10^6 cells in 50 μl of CLM/well). After centrifugation, fluorescence from the luminal indicator was recorded using a FlexStation II platereader (Molecular Devices) equipped to allow automated additions [39]. In all experiments, the intracellular stores were allowed to load to steady-state with Ca^{2+} after addition of MgATP. IP_3 was then added with thapsigargin (1 μM, to inhibit Ca^{2+} reuptake). The Ca^{2+} release evoked by IP_3 is expressed as a fraction of the ATP-dependent Ca^{2+} uptake.

Patch-clamp recording

Currents were recorded from patches excised from the outer nuclear envelope of DT40 cells expressing recombinant rat IP_3R1 using symmetrical caesium methanesulfonate (140 mM) as the charge-carrier. The composition of recording solutions and methods of analysis were otherwise as described previously [40].

Expression of N-terminal fragments of IP_3R

The pTrcHis constructs were used for expression of N-terminally His_6-tagged proteins in *Escherichia coli* strain BL21(DE3) cells. Before use for $[^3H]IP_3$ binding, proteins were cleaved from the His_6 tags using biotinylated thrombin (Novagen) at the engineered thrombin-cleavage site [33]. Complete cleavage was verified by Western blotting using an anti-His_6 antibody. The proteins were used for $[^3H]IP_3$ binding without further purification [33].

$[^3H]IP_3$ binding

Equilibrium-competition binding assays were performed at 4 °C for 5 min in CLM (500 μl) with a free Ca^{2+} concentration of 220 nM and containing $[^3H]IP_3$ (0.75–1.5 nM), bacterial lysate (10 μg of protein for IBC and 100 μg of protein for NT) or cerebellar membranes (50 μg of protein) and competing ligands. Non-specific binding was defined by addition of 10 μM IP_3. Bound and free $[^3H]IP_3$ were separated by centrifugation at 20 000 ***g*** for 5 min, after addition of poly(ethylene glycol) (15 % final concentration) and γ-globulin (0.75 mg) for soluble proteins. Results were analysed by fitting to a Hill equation (using GraphPad Prism) from which the IC_{50} (half-maximal inhibitory concentration) and thereby the K_d (equilibrium dissociation constant) were calculated [33].

Western blotting

Cells in Ca^{2+}-free CLM containing 2-mercaptoethanol (1 mM) and protease inhibitors were lysed by addition of PopCulture (10 %), lysozyme (10 μg/ml), DNAse (5 units/ml) and RNAse (10 μg/ml). The proteins were separated using SDS/PAGE pre-cast mini-gels (Invitrogen) and transferred on to a PVDF membrane using an Iblot dry-transfer apparatus (Invitrogen). The primary antibodies were rabbit anti-His_6 (1:3000 dilution) (Sigma) and anti-IP_3R1 (1:1000 dilution) [33]. HRP (horseradish peroxidase)-conjugated anti-rabbit secondary antibodies (1:5000 dilution) (AbCam) and the Super Signal West Pico chemiluminescence reagent (Pierce) were used to detect immunoreactivity. Bands were quantified using GeneTools software (Syngene).

Statistical analysis

For comparisons of K_d, EC_{50} (half-maximally effective concentration) or IC_{50} values, their negative logarithms (pK_d, pEC_{50} and pIC_{50}; means $\pm$ S.E.M.) were used for statistical analyses. For clarity, some Figures show normalized results, but all statistical analyses were performed on the raw data using

paired or unpaired Student's t tests. $P < 0.05$ was considered significant.

RESULTS AND DISCUSSION

Reversible inhibition of IP_3-evoked Ca^{2+} release by an endogenous 1-8-14 peptide

A sequence within the SD of all known IP_3Rs (residues 53–66 in rat IP_3R1; Supplementary Figure S1 at http://www.biochemj.org/bj/449/bj4490039add.htm) includes the critical hydrophobic residues of a 1-8-14 CaM-binding motif appropriately oriented within the known structure of the SD [41] (Figures 1B and 1C) and with the required net positive charge [35]. The sequence lies within one of the two regions (residues 49–81; Figure 1A) within the NT reported to bind CaM [42] and CaBP1 [14]. A similar sequence is present within the N-terminal of all RyRs (Supplementary Figure S1). To test our hypothesis that inhibition of IP_3R by MLCK peptide results from disruption of an essential interaction involving an endogenous 1-8-14 motif, we assessed the effects of a peptide derived from this motif (1-8-14 peptide; Figure 1B and Supplementary Table S1) on IP_3-evoked Ca^{2+} release.

The 1-8-14 peptide inhibited IP_3-evoked Ca^{2+} release via IP_3R1 without affecting either Ca^{2+} uptake or the sensitivity (EC_{50}) to IP_3 (Figures 2A–2D). A maximally effective concentration of the peptide reduced the maximal response to IP_3 by $77 \pm 7\,\%$. The IC_{50} for 1-8-14 peptide was 767 μM (pIC_{50}, 3.1 ± 0.25) (Figure 2C). Neither a mutant 1-8-14 peptide, in which two critical hydrophobic residues are mutated (1-8-14^C, 3 mM) nor a scrambled peptide (1-8-14^S, 3 mM) had any effect on IP_3-evoked Ca^{2+} release (Figure 2C). Both MLCK peptide (isoelectric point, pI 14.0) and 1-8-14 peptide (pI 11.6) are very basic and might therefore have inhibited IP_3-evoked Ca^{2+} release by binding directly to IP_3. We demonstrated previously that this was not the case for MLCK peptide [35], and it is also unlikely for the 1-8-14 peptide. The 1-8-14 and 1-8-14^S peptides are equally basic, but only the former inhibited IP_3R; the percentage inhibition caused by 3 mM 1-8-14 peptide is similar for all IP_3 concentrations ($\sim$75 %), and neither was the inhibition reduced by increasing the IP_3 concentration beyond that required to stimulate maximal Ca^{2+} release (Figure 2B). We conclude that 1-8-14 peptide inhibits IP_3-evoked Ca^{2+} release by binding to IP_3R.

The 1-8-14 peptide is only 16 residues long. A longer peptide (30 residues, 1-8-14^L), which includes additional N- and C-terminal residues that are conserved in all IP_3Rs (Figure 1B and Supplementary Figure S1), also inhibited IP_3-evoked Ca^{2+} release without affecting Ca^{2+} uptake (Figure 2D). Although IP_3R may be slightly more sensitive to the longer peptide (IC_{50}, 326 μM; pIC_{50}, 3.5 ± 0.25) than to the 1-8-14 peptide (767 μM, 3.1 ± 0.25); the difference was not statistically significant. Subsequent studies used the shorter 1-8-14 peptide because it was less expensive.

The results shown in Figure 2(E) demonstrate that the effects of a maximally effective concentration of 1-8-14 peptide (3 mM) are fully reversible. These experiments, which require extensive washing of the cells between successive challenges with the peptide, confirm that the inhibition of IP_3Rs by the 1-8-14 peptide, like that by MLCK peptide [35], does not result from dissociation of CaM from IP_3R [36]. Our previous study demonstrated that MLCK peptide more potently inhibited IP_3R when the cytosolic free Ca^{2+} concentration was increased [35]. Similar results were obtained with 1-8-14 peptide (Figure 2F). We conclude that 1-8-14 peptide inhibits IP_3-evoked Ca^{2+} release by binding to the IP_3R and the inhibition is enhanced at elevated cytosolic Ca^{2+} concentrations.

Inhibition of single-channel currents through IP_3Rs by 1-8-14 peptide

In patch-clamp recordings from the nuclear envelope of DT40 cells expressing rat IP_3R1, a maximally effective concentration of IP_3 stimulated IP_3R activity and this was massively attenuated by the 1-8-14 peptide (3 mM) (Figures 3A and 3B). Our results are consistent with the peptide causing a 50 % decrease in the mean channel open time (τ_o) (Figure 3C). However, the overall channel activity (NP_o) was so low under these conditions that we cannot reliably estimate the number of active IP_3Rs (N) within each patch. We cannot therefore entirely eliminate the possibility that each patch fortuitously included several IP_3Rs and that their clustering caused τ_o to fall from $\sim$10 ms to $\sim$5 ms as we reported previously [40]. An effect on τ_o would be unusual because most regulators of IP_3Rs affect the duration of closed states (τ_c) [6,40]. The effect of the peptide on τ_o is not, however, sufficient to account for the $\sim$10-fold decrease in NP_o (Figure 3A), suggesting that the 1-8-14 peptide must also affect the rate of channel opening (i.e. τ_c). Because it was impossible to determine the number of active IP_3Rs in the presence of 1-8-14 peptide (see above), we could not reliably determine τ_c. The single-channel conductance (γ_{Cs}) was unaffected by 1-8-14 peptide: it was 214 ± 6 pS ($n = 3$) and 209 ± 6 pS ($n = 3$) for control and peptide-treated IP_3Rs respectively (Figure 3D).

These results establish that a peptide derived from an endogenous 1-8-14 motif within the SD of the IP_3R is similar to MLCK peptide in causing substantial and reversible inhibition of IP_3Rs that is independent of CaM. This conclusion is consistent with our suggestion that MLCK peptide inhibits IP_3Rs by mimicking an endogenous 1-8-14 motif, and so perhaps 'unzipping' an interdomain interaction [43] that is essential for activation of IP_3Rs.

1-8-14 peptide uncouples IP_3 binding from activation of IP_3Rs

Removal of the SD increases the affinity of both full-length IP_3Rs and the NT for IP_3 [33]. We [33] have suggested that this reflects the use of binding energy to drive conformational rearrangement of SD-IBC interfaces during the initial steps of IP_3R activation [5,44].

1-8-14 peptide (3 mM) increased specific binding of $[^3H]IP_3$ to full-length IP_3R1. Similar results were obtained with the NT, but IP_3 binding to the IBC was unaffected (Figure 4A). The latter demonstrates that 1-8-14 peptide does not interact directly with either the IP_3-binding site or with IP_3. Neither the mutated (1-8-14^C) nor scrambled (1-8-14^S) peptide had any effect on IP_3 binding to the NT (Figure 4A). These results with IP_3R fragments expressed in *E. coli*, which lack CaM, also further support our conclusion that the effects of 1-8-14 peptide are entirely independent of CaM.

Comparison of the effects of 1-8-14 peptide on stimulating $[^3H]IP_3$ binding to the NT (EC_{50}, 615 μM; pEC_{50}, 3.21 ± 0.19) (Figure 4B) with its inhibitory effect on IP_3-evoked Ca^{2+} release (IC_{50}, 767 μM; pIC_{50}, 3.1 ± 0.25) (Figure 2C) demonstrates that each is similarly sensitive to the peptide. These results are consistent with our hypothesis that the 1-8-14 peptide disrupts an interaction between the SD and IBC that is essential for IP_3R activation. The peptide thereby inhibits IP_3-evoked Ca^{2+} release (Figure 2) and IP_3R activity (Figure 3) and, by uncoupling IP_3 binding from subsequent conformational changes, it stimulates

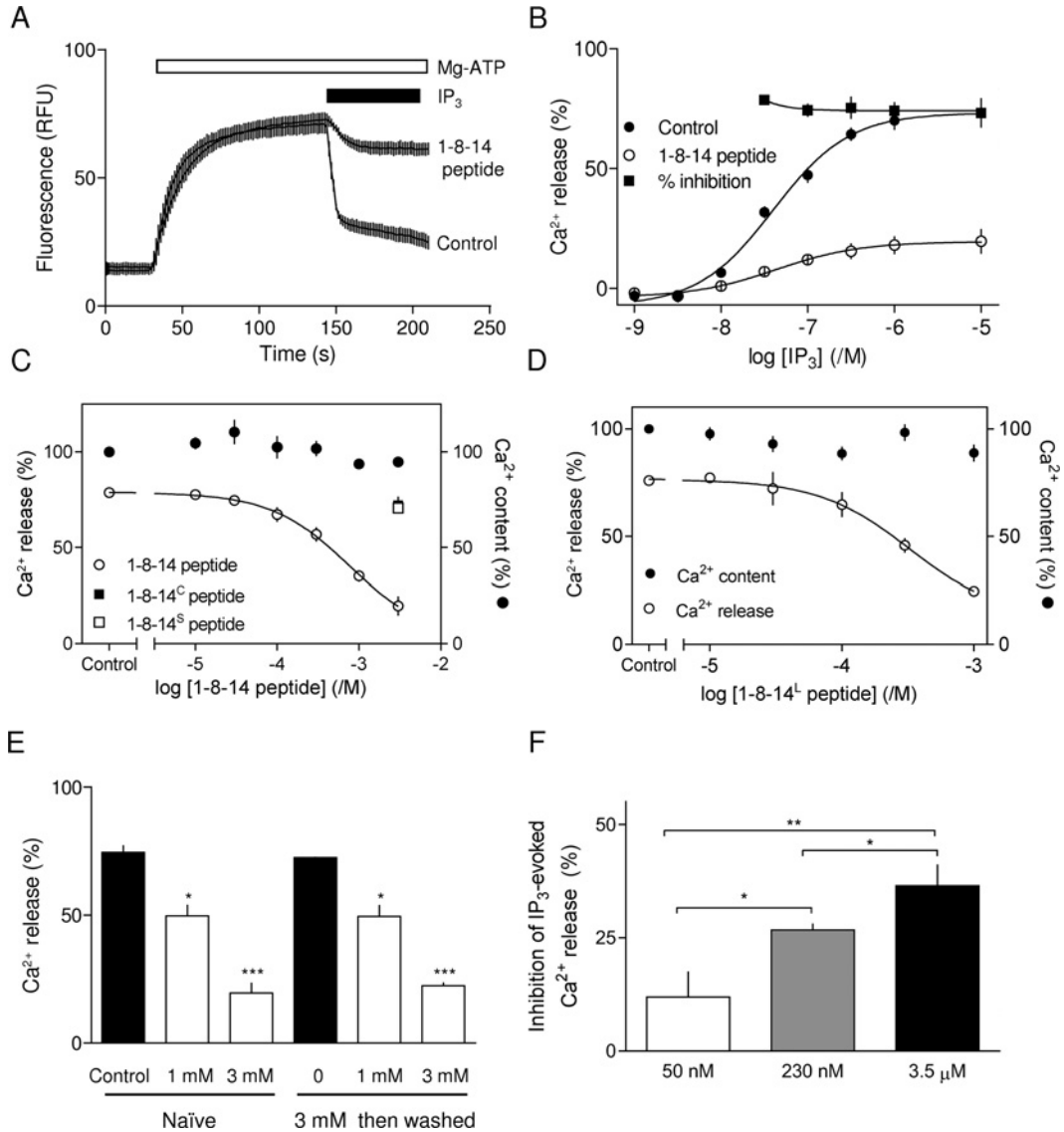

Figure 2 Inhibition of IP_3R by 1-8-14 peptide

(**A**) Typical recording of the free Ca^{2+} concentration within the endoplasmic reticulum of a population of permeabilized DT40-IP_3R1 cells showing Ca^{2+} uptake after addition of MgATP (1.5 mM), release of Ca^{2+} after addition of IP_3 (10 μM, with 1 μM thapsigargin to inhibit Ca^{2+} re-uptake) and inhibition of that release by 1-8-14 peptide (3 mM, present throughout as indicated, upper trace). Results are means $\pm$ S.E.M. for three replicates from a single experiment. (**B**) Concentration-dependent release of intracellular Ca^{2+} stores by IP_3 alone or after pre-incubation for 2.5 min with 1-8-14 peptide (3 mM). Inhibition by 1-8-14 peptide at each IP_3 concentration is also shown (%). 1-8-14 peptide caused a significant decrease in the maximal response ($P < 0.001$) without significantly changing the sensitivity to IP_3. (**C** and **D**) Permeabilized cells pre-incubated for 10–20 min with the indicated concentrations of peptide were stimulated with IP_3 (10 μM, in the continued presence of peptide). Results show the Ca^{2+} content of the stores before addition of IP_3, and the Ca^{2+} release evoked by IP_3. (**E**) Permeabilized cells were incubated alone or with 1-8-14 peptide (3 mM) for 10–20 min, washed and then resuspended in CLM. Ca^{2+} release by IP_3 (10 μM) was then measured after a further incubation for 10–20 min with the indicated concentrations of 1-8-14 peptide. The Ca^{2+} release evoked by IP_3 with and without peptide is shown for naive cells and after the pre-treatment with 3 mM peptide. The results establish that the effects of 1-8-14 peptide are fully reversible. (**F**) Permeabilized cells pre-incubated with or without 1-8-14 peptide (1 mM) for 10–20 min were stimulated with a maximally effective concentration of IP_3 in the continued presence of peptide in CLM with the indicated free Ca^{2+} concentration. Results show the inhibition of IP_3-evoked Ca^{2+} release (%) by 1-8-14 peptide at each free Ca^{2+} concentration. Results in (**B**)–(**F**) are means $\pm$ S.E.M. ($n \geqslant 3$). $^*P<0.05$, $^{**}P<0.01$ and $^{***}P<0.001$.

IP_3 binding (Figure 4). Subsequent experiments used mutagenesis of residues within the endogenous 1-8-14 motif to test this hypothesis further.

Mutations within the endogenous 1-8-14 sequence increase IP_3-binding affinity

If, as we suggest, the 1-8-14 peptide disrupts an essential interaction between the endogenous 1-8-14 sequence and another domain within the NT, we might expect mutation of appropriate residues in the SD to both disrupt IP_3R activation and increase IP_3-binding affinity. We tested the latter prediction by examining IP_3 binding to the NT in which each of the critical (1, 8 and 14) hydrophobic/aromatic residues that are important for Ca^{2+}–CaM binding to 1-8-14 motifs [45] was replaced with a charged hydrophilic residue (glutamate). The same hydrophobic residues are essential for MLCK [35] and 1-8-14 (Figure 2C) peptides to disrupt IP_3R activation.

NTs of IP_3R1 with point mutations in positions equivalent to the 1- (F53E), 8- (L60E) or 14-position (Y66E) of the

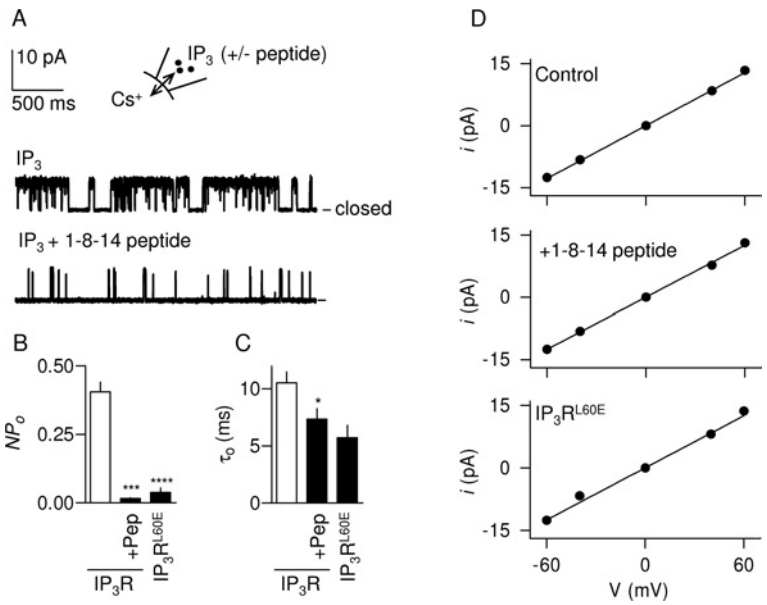

Figure 3 Inhibition of IP_3R gating by 1-8-14 peptide

(**A**) Typical recordings from excised nuclear patches stimulated with IP_3 (10 μM) with and without 1-8-14 peptide (3 mM) in the pipette solution. The holding potential was $+40$ mV. The closed state is shown. (**B** and **C**) NP_o (**B**) and τ_o (**C**) for IP_3R stimulated with IP_3 alone or with 1-8-14 peptide (3 mM, + Pep). Results for IP_3R^{L60E} are also shown. $^*P<0.05$, $^{***}P<0.001$ and $^{****}P<0.0001$ relative to native IP_3R without peptide. (**D**) Single-channel current (i)–voltage (V) relationships for the three stimulation conditions. Results in (**B**)–(**D**) are means $\pm$ S.E.M. ($n \geqslant 3$).

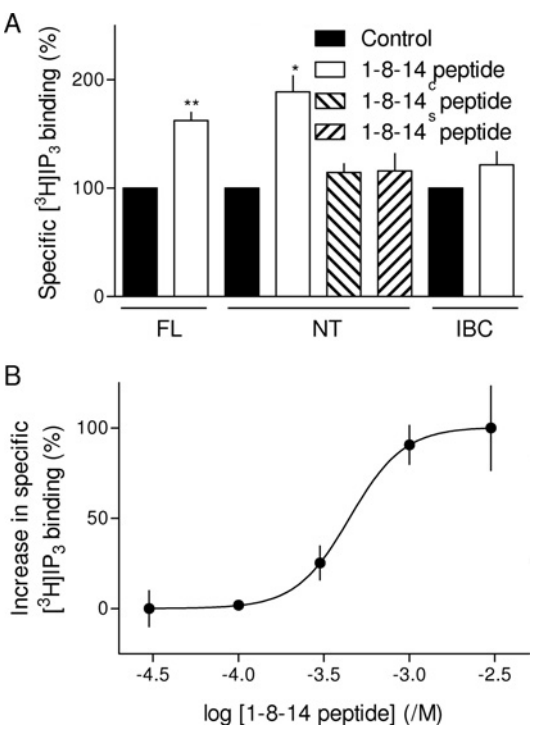

Figure 4 1-8-14 peptide directly stimulates IP_3 binding to the NT of IP_3R

(**A**) Specific equilibrium binding of $[^3H]IP_3$ (1.5 nM) to membranes from rat cerebellum (full-length IP_3R, FL) or to isolated NT or IBC, alone or in the presence of 3 mM of the indicated peptide. $^*P<0.05$ and $^{**}P<0.01$ relative to control; comparisons were performed on the raw data. (**B**) Concentration-dependent effects of 1-8-14 peptide on specific $[^3H]IP_3$ binding to NT in CLM with 220 nM free Ca^{2+} concentration, plotted as the increase in specific $[^3H]IP_3$ binding as a percentage of that evoked by the maximal concentration of peptide. Results are means $\pm$ S.E.M. ($n \geqslant 3$).

endogenous 1-8-14 motif (Figure 1A) were expressed in *E. coli*. Expression levels of the NT and its mutants were not identical (Figure 5A), but they were each sufficient to allow the affinity for IP_3 and the effects of peptides to be determined after cleavage of the His_6 tag, but without further purification [33]. As expected, IP_3 bound to the IBC with greater affinity (17-fold) than to the NT (Figure 5B) [33,46,47], consistent with our suggestion that, in the absence of the SD, less binding energy is diverted into conformational changes [33]. Mutation of critical residues within the endogenous 1-8-14 motif significantly increased the affinity of the NT for IP_3 (Figure 5B and Table 1), although none was as effective as complete removal of the SD. This is consistent with our observation that neither the 1-8-14 (Figure 2) nor MLCK [35] peptide entirely inhibits IP_3-evoked Ca^{2+} release, whereas removal of the SD totally uncouples IP_3 binding from IP_3R activation [48]. Although maximally effective concentrations of MLCK (100 μM) or 1-8-14 (3 mM) peptides similarly increased IP_3 binding to the NT, neither peptide had any effect on $[^3H]IP_3$ binding to the NT with mutations in any of the critical 1-8-14 residues (Figures 5C and 5D). Mutation of a residue immediately preceding the critical 1-position of the 1-8-14 motif (K52E), which did not increase the affinity of IP_3 for the NT (Supplementary Figure S2A at http://www.biochemj.org/bj/449/bj4490039add.htm), had no effect on the responses to MLCK or 1-8-14 peptides (Figures 5C and 5D) and neither did it affect IP_3-evoked Ca^{2+} release [33] (Supplementary Figure S2B). These results establish that mutation of critical residues within the endogenous 1-8-14 motif selectively increases IP_3-binding affinity and these effects are non-additive with those of either MLCK or 1-8-14 peptide.

Mutations within the 1-8-14 motif selectively increase agonist affinity

Our hypothesis is that the apparent affinity of agonists (such as IP_3) for native IP_3Rs is reduced because some of their binding energy is diverted into the conformational changes that activate

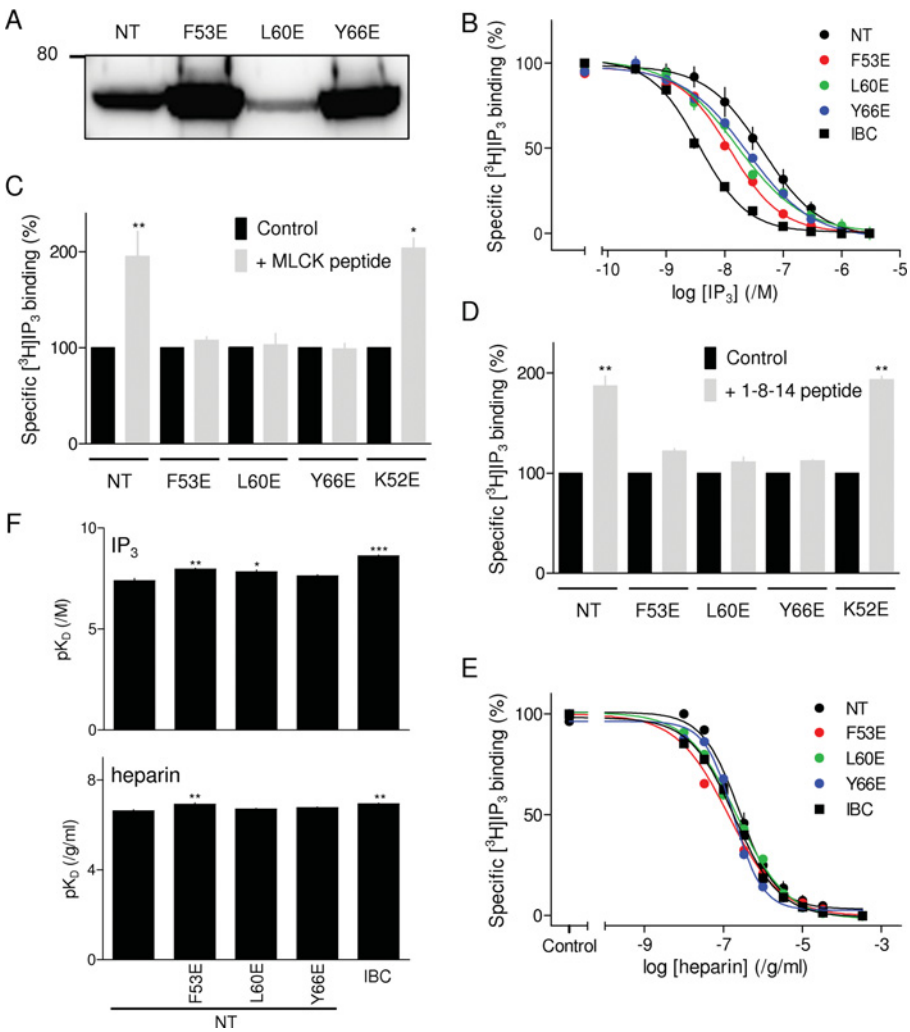

Figure 5 Mutations within the 1-8-14 motif mimic the effect of 1-8-14 peptide on IP_3 binding

(**A**) Western blot (typical of three independent experiments) with an anti-His_6 antibody of lysates (5 μg of protein/lane) from bacteria expressing NT with the indicated mutations. The 80 kDa molecular-mass marker is shown. (**B**) Concentration-dependent effect of IP_3 on specific [^{3}H]IP_3 binding to the IBC, NT and mutated NT. (**C** and **D**) Effects of MLCK peptide (**C**, 100 μM) and 1-8-14 peptide (**D**, 3 mM) on specific binding of [^{3}H]IP_3 (1.5 nM) to the NT and the indicated mutants (each expressed as a percentage of the control). (**E**) Specific binding of [^{3}H]IP_3 (1.5 nM) to the IBC, NT and mutated NT in the presence of the indicated concentrations of heparin. (**F**) Summary results from experiments similar to those in (**E**) showing the K_d for IP_3 and heparin binding to the IBC, NT and mutated NT. Results in (**B**)–(**F**) are means ± S.E.M. ($n \geqslant 3$). $^*P<0.05$, $^{**}P<0.01$ and $^{***}P<0.001$ relative to control; comparisons were performed on the raw data.

Table 1 Binding of IP_3 and heparin to N-terminal fragments of IP_3R1

Equilibrium competition binding using [^{3}H]IP_3 was used to measure the pK_d of IP_3 and heparin for the N-terminal fragments of IP_3R1. Affinities for ligands are also shown expressed as fold increase relative to wild-type NT (i.e. K_d^{NT}/K_d^{mutant}). Results are means ± S.E.M. ($n \geqslant 3$). $^*P < 0.05$, $^{**}P < 0.01$ and $^{***}P < 0.001$ relative to NT.

Fragment	pK_d, /M IP_3 (K_d, nM)	Affinity relative to NT	pK_d, /g/ml heparin (K_d, ng/ml)	Affinity relative to NT
NT	7.40 ± 0.11 (40.0)	1	6.62 ± 0.06 (239)	1
F53E	7.97 ± 0.05** (10.8)	4	6.92 ± 0.06** (120)	2
L60E	7.84 ± 0.08* (14.5)	3	6.70 ± 0.04 (200)	1.2
Y66E	7.64 ± 0.04 (22.8)	2	6.77 ± 0.03 (171)	1.4
IBC	8.62 ± 0.05*** (2.4)	17	6.93 ± 0.04** (117)	2.0

the IP_3R [33]. Antagonists, because they need not evoke the rearrangement of the IBC and SD that initiates IP_3R activation, may be less affected by disruption of these interactions. We therefore examined the effects of the SD and of point mutations within the endogenous 1-8-14 sequence on binding to the NT of heparin, a competitive antagonist of IP_3 [49]. The results demonstrate that, whereas removal of the SD increased the affinity of the NT for IP_3 17-fold, it caused only a 2-fold increase in the affinity for heparin. Point mutations within the endogenous 1-8-14 motif also caused larger increases in the affinity for IP_3 than for heparin (Figures 5E and 5F, and Table 1). These results are important because they demonstrate that the effects of the SD and of mutations within the 1-8-14 sequence on ligand binding are specific for an agonist of the IP_3R. They thereby demonstrate the importance of the 1-8-14 motif in specifically mediating activation of IP_3Rs.

Mutations within the endogenous 1-8-14 motif uncouple IP_3 binding from gating of IP_3Rs

It proved difficult to establish stable DT40 cell lines expressing rat IP_3R1 in which critical residues within the 1-8-14 motif were mutated, but we succeeded with two mutants (Figure 6A). The first (IP_3R^{L60E}) is mutated at the 8-position of the 1-8-14 motif

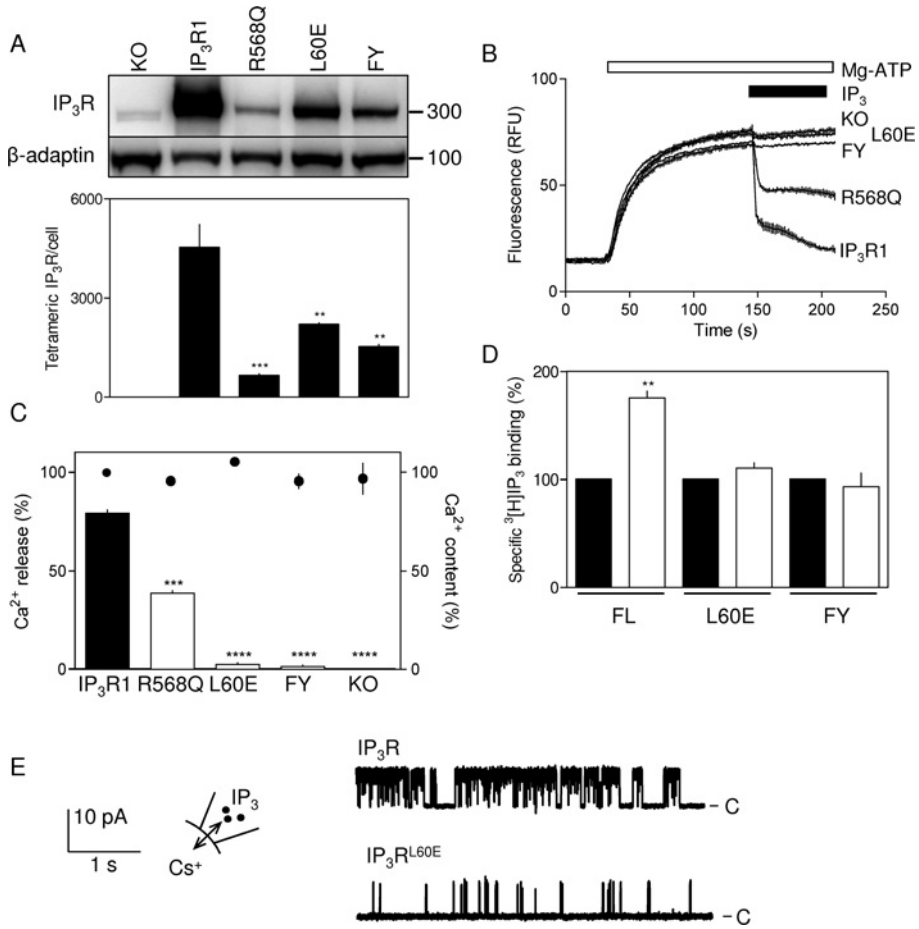

Figure 6 The endogenous 1-8-14 motif is essential for activation of IP_3R

(**A**) Expression of IP_3R1 in DT40 cells stably expressing each of the indicated mutants. Each lane was loaded with 4×10^3 cells and probed with antisera to IP_3R1 (upper panel) or β-adaptin (lower panel). The R568Q mutant (which reduces the affinity of the IP_3R for IP_3) [50] is shown because it provides a control for functional assays of cells expressing IP_3R at low density. Molecular-mass markers are shown on the right. The Western blot is typical of three independent experiments. The lower panel shows summary results (means $\pm$ S.E.M., $n=3$), where IP_3R expression was calculated from blots that included DT40-IP_3R1 membranes in which levels of expression were established by equilibrium competition [^{3}H]IP_3 binding. (**B**) Typical responses to IP_3 (10 μM) from DT40 cells lacking IP_3R (KO) or expressing wild-type IP_3R1 or IP_3R with the indicated mutations (see the text for details). (**C**) Summary results show the Ca^{2+} content of the loaded stores (●) and the Ca^{2+} released by IP_3 (histograms) for each of the indicated cell lines. (**D**) Specific [^{3}H]IP_3 binding (1.5 nM) to full-length IP_3R (FL) with the indicated mutations (L60E or FY, see the text for details) in permeabilized DT40 cells alone or in the presence of 100 μM MLCK peptide. Results in (**C**) and (**D**) are means $\pm$ S.E.M. ($n\geqslant3$). (**E**) Typical records from active excised nuclear patches of DT40 cells expressing IP_3R1 or IP_3R1^{L60E} stimulated with IP_3 (10 μM). The holding potential was $+40$ mV. C denotes the closed state. Summary data are provided in Figures 3(B)–3(D). $^{**}P<0.01$, $^{***}P<0.001$ and $^{****}P<0.0001$ relative to IP_3R1 (**A** and **C**) or control (**D**).

and the second has mutations at both the 1- (F53E) and 14-positions (Y66E) (IP_3R^{FY}). As expected, a maximally effective concentration of IP_3 (10 μM) failed to stimulate Ca^{2+} release from permeabilized DT40 cells lacking IP_3R (DT40-KO cells) [37,40], but it caused release of 81 ± 1 % of the Ca^{2+} stores of DT40-IP_3R1 cells (Figures 6B and 6C). In the cell lines expressing IP_3R with a mutated 1-8-14 motif, there was barely detectable Ca^{2+} release that was not significantly different from that observed in DT40-KO cells (Figures 6B and 6C). ATP-dependent Ca^{2+} uptake into the ER was similar for each cell line (Figure 6C). We were concerned that the lower level of expression of mutant IP_3R relative to wild-type ($\sim$30–50 %, Figure 6A) might have contributed to the lack of detectable IP_3-evoked Ca^{2+} release. However, in another stable DT40 cell line where the IP_3-binding site was mutated (R568Q), causing a $\sim$10-fold decrease in IP_3 affinity [50], IP_3R expression ($\sim$15 % of wild-type) was less than half that of the cell lines with mutations in the 1-8-14 motif (Figure 6A). Nevertheless, IP_3 caused a readily detectable release of Ca^{2+} from the intracellular stores of DT40-IP_3R^{R568Q} cells (49 ± 2 % of that detected in DT40-IP_3R1 cells) (Figures 6B and 6C). We conclude that the lack of detectable Ca^{2+} release in cells expressing IP_3R with a mutant 1-8-14 motif is not attributable to reduced IP_3R expression. Neither is it likely that the lack of response to IP_3 from mutant IP_3R reflects a more global disruption of IP_3R structure because each of the full-length mutant IP_3Rs bound IP_3, although, as predicted, addition of MLCK peptide increased IP_3 binding to only the wild-type IP_3R (Figure 6D). Furthermore, DT40 cells expressing IP_3R1 with a mutation in an adjacent residue (DT40-IP_3R1^{K52E}) responded normally to IP_3 [33] (Supplementary Figure S2B). These results are consistent with the suggestion that mutations within the endogenous 1-8-14 motif mimic addition of exogenous MLCK peptide by uncoupling IP_3 binding from the conformational changes that lead to opening of the IP_3R pore. Single-channel analyses provide further support for this conclusion.

Yamazaki et al. [51] reported recently the functional effects of mutations within IP_3R including some within the 1-8-14 motif (F53D and Y66A). We note, however, that some of their

mutations, e.g. Y167A, which is clearly implicated in IP_3R activation, abolished IP_3-evoked Ca^{2+} release from microsomes without affecting Ca^{2+} signals evoked by activation of the BCR (B-cell receptor) in intact cells. This unexplained disparity casts some doubt over whether in these assays responses from intact cells faithfully report the activity of IP_3R. In DT40 cells expressing an IP_3R with five mutations that included Y66A (the 14-position of the 1-8-14 motif), activation of the BCR evoked a Ca^{2+} signal, suggesting that the mutant IP_3R was functional [51]. However, in this IP_3R, the mutant had one hydrophobic residue replaced by another and this might not radically affect the behaviour of the 1-8-14 motif. In preliminary analyses of cells expressing IP_3Rs in which the first position of the 1-8-14 motif was mutated (F53D), Ca^{2+} signals were also observed after activation of the BCR [51]. This may reflect a limitation of the BCR-based assay (see above) or it may provide evidence for a lesser role of the 1-position in the 1-8-14 motif. We have not succeeded in establishing a DT40 cell line expressing IP_3Rs with only this mutation, although our results do clearly show that IP_3Rs with mutations in both the 1- and 14-positions (IP_3R^{FY}) are barely responsive to IP_3 (Figure 6).

Mutation of the endogenous 1-8-14 motif attenuates IP_3R gating without affecting single-channel conductance

In keeping with the reduced expression of IP_3R^{L60E} in DT40 cells (Figure 6A), the frequency with which functional IP_3Rs were detected in excised nuclear patches was much lower for nuclei from paired experiments with DT40-IP_3R1^{L60E} cells (three of 48 patches) than from DT40-IP_3R1 cells (five of 13 patches). In parallel analyses, functional IP_3Rs were never detected in DT40-KO cells (none of 30 patches). The single-channel conductances (γ_{Cs}) of the mutant IP_3R^{L60E} (209 ± 8 pS) and normal IP_3R (214 ± 6 pS) were indistinguishable (Figure 3D), but NP_o was massively decreased in the mutant (Figures 3B and 6E). Our interpretation of the latter is, as we described in our analyses of the 1-8-14 peptide, limited by our inability, when NP_o is so low for IP_3R1^{L60E}, to estimate reliably the number of active IP_3R within a patch. Nevertheless, it is clear that the major effect on single-channel behaviour of mutating the endogenous 1-8-14 motif of IP_3R1 (Figures 3B–3D and 6E) and of adding 1-8-14 peptide to normal IP_3R1 (Figure 3) is similar: both decrease NP_o without affecting γ_{Cs}. These results establish that mutations in the endogenous 1-8-14 motif or addition of 1-8-14 peptide uncouple ligand binding from channel gating without compromising the behaviour of the pore.

Conclusions: interactions between endogenous 1-8-14 and CaM-like motifs mediate activation of IP_3Rs

CaM [22] or related EF-hand-containing proteins [14,25], peptides that comprise 1-8-14 CaM-binding motifs [35,36] (Figures 2–4) or disruption of a conserved endogenous 1-8-14-like motif within the SD of IP_3Rs inhibit IP_3-evoked Ca^{2+} release (Figures 5 and 6) by massively reducing NP_o of IP_3R (Figures 3 and 6E). We conclude that an endogenous 1-8-14 motif within the SD (Figure 1) is essential for IP_3R activation. Where it has been examined, the inhibitory proteins or peptides are more potent when Ca^{2+} is bound to the IP_3R [26,35] (Figure 2F). We therefore speculate that the endogenous 1-8-14 motif may interact with an unidentified domain that includes an EF-hand-like structure and that these interactions might be related to Ca^{2+} regulation of IP_3R (Figure 7). We suggest that competing peptides (CaM-like or 1-8-14 motifs) or mutagenesis of the endogenous 1-8-14 motif inhibit IP_3Rs by disrupting this essential interaction in a manner

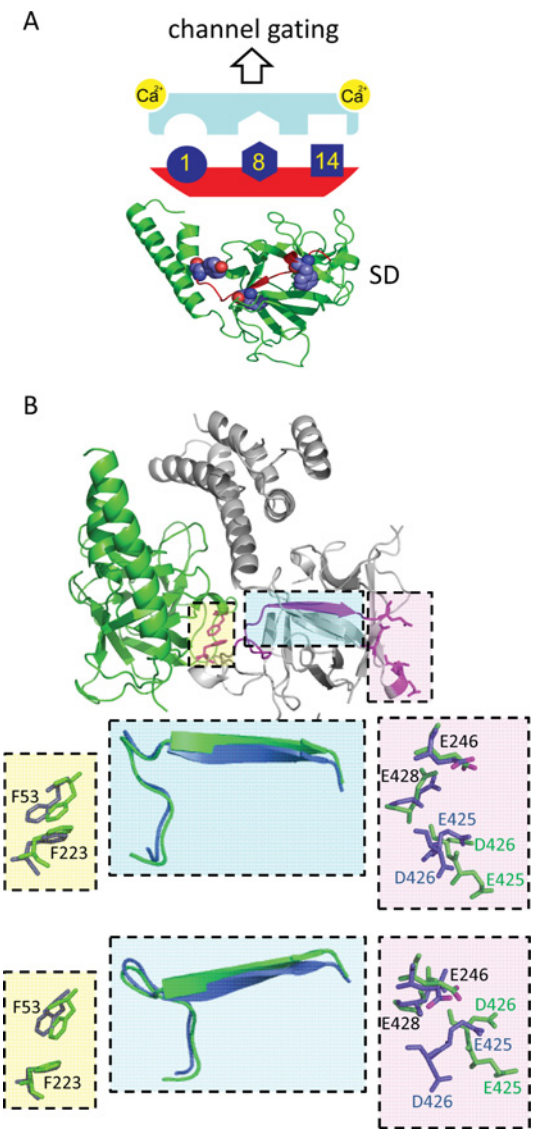

Figure 7 Activation of IP_3Rs requires an endogenous 1-8-14 motif

IP_3 binding to the IBC initiates conformational changes that pass via the SD and lead, via regulation of Ca^{2+} binding to the IP_3R, to opening of the pore [33]. (**A**) An endogenous 1-8-14 motif within the SD is essential for IP_3R activation. We speculate (upper panel) that interaction of this CaM-binding motif (red, conserved hydrophobic residues in dark blue) with an endogenous, but presently unknown, CaM-like structure (pale blue) within the NT may link IP_3 binding to Ca^{2+} binding. (**B**) Another possibility is that IP_3 binding rearranges the 1-8-14 motif and so repositions a critical acidic residue (Glu^{246}) that may then contribute to a Ca^{2+}-binding site (Ca-1) [55]. The NT without IP_3 bound (PDB code 3UJ0) [5] is shown with the IBC in grey and the SD in green to highlight Phe^{53} (within the 1-8-14 motif) and Phe^{223} to which it is closely apposed (yellow box), residues proposed to form the Ca-1 site (pink box) and the β-sheet that links Phe^{223} to Glu^{246} (cyan box). The expanded views (each rotated to show key movements) show the critical residues and the linking β-sheet before (green) and after IP_3 binding (blue, PDB code 3UJ4). The carboxy oxygen atoms in Glu^{246} are shown in magenta. We speculate that separation of Phe^{53} and Phe^{223} when IP_3 binds is associated with twisting of the linking β-sheet and movement of Glu^{246} towards three other acidic residues (Glu^{425}, Asp^{426} and Glu^{428}) and that they may then together form an effective Ca^{2+}-binding site.

similar to the 'unzipping' of interdomain interactions in RyRs [32,43,52]. The scheme is appealing because IP_3 regulates binding of Ca^{2+} to IP_3Rs and thereby leads to channel gating [34,53]. The identity of this Ca^{2+}-binding site is unknown. It is, however, clear that Ca^{2+} regulates IP_3 binding to the NT only when the SD is present [42], suggesting that a Ca^{2+}-binding site within the NT may be regulated by interactions between the SD and IBC. One

possibility is that an endogenous EF-hand-like structure might provide the Ca^{2+}-binding site and that its interaction with the 1-8-14 motif links IP_3 and Ca^{2+} binding (Figure 7A). Bioinformatic analyses had suggested the presence of two possible EF-hand-like structures within the IBC [9,54], but neither is evident in high-resolution structures of the IBC [55] and NT [5,56]. Neither have we succeeded in identifying a complementary partner of the 1-8-14 motif. Another possibility is suggested by comparison of the structures of the NT with and without IP_3 bound [5,56], which reveal that Phe^{53} (the first hydrophobic residue of the 1-8-14 motif) and Phe^{223} are closely apposed ($\sim$3.9 Å; 1 Å = 0.1 nm), but they move apart ($\sim$5.3 Å) when IP_3 binds (Figure 7B). A β-sheet links Phe^{223} to Glu^{246}, and the movement of Phe^{223} is associated with a repositioning of an acidic residue in the β-domain of the IBC (Glu^{246}). This brings Glu^{246} closer to three other acidic residues (Glu^{425}, Asp^{426} and Glu^{428}). The rearrangement is interesting because these four residues have been proposed to form a Ca^{2+}-binding site (Ca-I) [55]. Furthermore, a peptide (residues 378–450) that includes most of these residues binds Ca^{2+}, and the binding is abolished by mutation of the acidic residues [42]. A second possibility is therefore that IP_3-evoked movement of the critical 1-8-14 motif contributes to formation of an effective Ca^{2+}-binding site within the IBC by bringing a fourth acidic residue into appropriate association with three others.

We conclude that a conserved 1-8-14 motif within the SD is essential for IP_3R activation and speculate that its interaction with either an endogenous CaM-like motif or acidic residues within the IBC may link IP_3 and Ca^{2+} binding. Inhibition of IP_3R by CaM and related proteins probably results from disruption of this essential interaction.

AUTHOR CONTRIBUTION

Yi Sun and Ana Rossi performed the Ca^{2+}-release and IP_3-binding analyses. Taufiq Rahman performed the single-channel analyses. Colin Taylor directed the study, and with input from all authors, wrote the paper.

FUNDING

Supported by the Wellcome Trust [grant number 085295], Biotechnology and Biological Sciences Research Council [grant number BB/H009736/1] and a studentship from the Engineering and Physical Sciences Research Council (to Y.S.). A.R. is a fellow of Queens' College, Cambridge. T.R. is a Drapers Research Fellow of Pembroke College, Cambridge.

REFERENCES

1 Berridge, M. J., Lipp, P. and Bootman, M. D. (2000) The versatility and universality of calcium signalling. Nat. Rev. Mol. Cell Biol. **1**, 11–21
2 Tadross, M. R., Dick, I. E. and Yue, D. T. (2008) Mechanism of local and global Ca^{2+} sensing by calmodulin in complex with a Ca^{2+} channel. Cell **133**, 1228–1240
3 Marchant, J. S. and Parker, I. (2001) Role of elementary Ca^{2+} puffs in generating repetitive Ca^{2+} oscillations. EMBO J. **20**, 65–76
4 Hamilton, S. L. and Serysheva, I. I. (2009) Ryanodine receptor structure: progress and challenges. J. Biol. Chem. **284**, 4047–4051
5 Seo, M.-D., Velamakanni, S., Ishiyama, N., Stathopulos, P. B., Rossi, A. M., Khan, S. A., Dale, P., Li, C., Ames, J. B., Ikura, M. and Taylor, C. W. (2012) Structural and functional conservation of key domains in InsP_3 and ryanodine receptors. Nature **483**, 108–112
6 Foskett, J. K., White, C., Cheung, K. H. and Mak, D. O. (2007) Inositol trisphosphate receptor Ca^{2+} release channels. Physiol. Rev. **87**, 593–658
7 Zalk, R., Lehnart, S. E. and Marks, A. R. (2007) Modulation of the ryanodine receptor and intracellular calcium. Annu. Rev. Biochem. **76**, 367–385
8 Chen, S. R. W. and MacLennan, D. H. (1994) Identification of calmodulin-, Ca^{2+}- and ruthenium red-binding domains in the Ca^{2+} release channel (ryanodine receptor) of rabbit skeletal muscle sarcoplasmic reticulum. J. Biol. Chem. **269**, 22698–22704
9 Sienaert, I., Missiaen, L., De Smedt, H., Parys, J. B., Sipma, H. and Casteels, R. (1997) Molecular and functional evidence for multiple Ca^{2+}-binding domains on the type 1 inositol 1,4,5-trisphosphate receptor J. Biol. Chem. **272**, 25899–25906
10 Fessenden, J. D., Feng, W., Pessah, I. N. and Allen, P. D. (2004) Mutational analysis of putative calcium binding motifs within the skeletal ryanodine receptor isoform, RyR1. J. Biol. Chem. **279**, 53028–53035
11 Miyakawa, T., Mizushima, A., Hirose, K., Yamazawa, T., Bezprozvanny, I., Kurosaki, T. and Iino, M. (2001) Ca^{2+}-sensor region of IP_3 receptor controls intracellular Ca^{2+} signaling. EMBO J. **20**, 1674–1680
12 Chin, D. and Means, A. R. (2000) Calmodulin: a prototypical calcium sensor. Trends Cell Biol. **10**, 322–328
13 Wright, N. T., Prosser, B. L., Varney, K. M., Zimmer, D. B., Schneider, M. F. and Weber, D. J. (2008) S100A1 and calmodulin compete for the same binding site on ryanodine receptor. J. Biol. Chem. **283**, 26676–26683
14 Nadif Kasri, N., Holmes, A. M., Bultynck, G., Parys, J. B., Bootman, M. D., Rietdorf, K., Missiaen, L., McDonald, F., De Smedt, H., Conway, S. J. et al. (2004) Regulation of InsP_3 receptor activity by neuronal Ca^{2+}-binding proteins. EMBO J. **23**, 312–321
15 Michikawa, T., Hirota, J., Kawano, S., Hiraoka, M., Yamada, M., Furuichi, T. and Mikoshiba, K. (1999) Calmodulin mediates calcium-dependent inactivation of the cerebellar type 1 inositol 1,4,5-trisphosphate receptor. Neuron **23**, 799–808
16 Nosyreva, E., Miyakawa, T., Wang, Z., Glouchankova, L., Iino, M. and Bezprozvanny, I. (2002) The high-affinity calcium–calmodulin-binding site does not play a role in the modulation of type 1 inositol 1,4,5-trisphosphate receptor function by calcium and calmodulin. Biochem. J. **365**, 659–667
17 Zhang, X. and Joseph, S. K. (2001) Effect of mutation of a calmodulin-binding sites on Ca^{2+} regulation of inositol trisphosphate receptors. Biochem. J. **360**, 395–400
18 Taylor, C. W. and Laude, A. J. (2002) IP_3 receptors and their regulation by calmodulin and cytosolic Ca^{2+}. Cell Calcium **32**, 321–334
19 Rodney, G. G., Moore, C. P., Williams, B. Y., Zhang, J.-Z., Krol, J., Pedersen, S. E. and Hamilton, S. L. (2001) Calcium binding to calmodulin leads to an N-terminal shift in its binding site on the ryanodine receptor. J. Biol. Chem. **276**, 2069–2074
20 Yamaguchi, N., Takahashi, N., Xu, L., Smithies, O. and Meissner, G. (2007) Early cardiac hypertrophy in mice with impaired calmodulin regulation of cardiac muscle Ca^{2+} release channel. J. Clin. Invest. **117**, 1344–1353
21 Missiaen, L., Parys, J. B., Weidema, A. F., Sipma, H., Vanlingen, S., De Smet, P., Callewaert, G. and De Smedt, H. (1999) The bell-shaped Ca^{2+}-dependence of the inositol 1,4,5-trisphosphate induced Ca^{2+} release is modulated by Ca^{2+}/calmodulin. J. Biol. Chem. **274**, 13748–13751
22 Adkins, C. E., Morris, S. A., De Smedt, H., Török, K. and Taylor, C. W. (2000) Ca^{2+}-calmodulin inhibits Ca^{2+} release mediated by type-1, -2 and -3 inositol trisphosphate receptors. Biochem. J. **345**, 357–363
23 Lin, C., Widjaja, J. and Joseph, S. K. (2000) The interaction of calmodulin with alternatively spliced isoforms of the type-I inositol trisphosphate receptor. J. Biol. Chem. **275**, 2305–2311
24 Yamada, M., Miyawaki, A., Saito, K., Yamamoto-Hino, M., Ryo, Y., Furuichi, T. and Mikoshiba, K. (1995) The calmodulin-binding domain in the mouse type 1 inositol 1,4,5-trisphosphate receptor. Biochem. J. **308**, 83–88
25 Li, C., Chan, J., Haeseleer, F., Mikoshiba, K., Palczewski, K., Ikura, M. and Ames, J. B. (2009) Structural insights into Ca^{2+}-dependent regulation of inositol 1,4,5-trisphosphate receptors by CaBP1. J. Biol. Chem. **284**, 2472–2481
26 Nadif Kasri, N., Bultynck, G., Smyth, J., Szlufcik, K., Parys, J., Callewaert, G., Missiaen, L., Fissore, R. A., Mikoshiba, K. and De Smedt, H. (2004) The N-terminal Ca^{2+}-independent calmodulin-binding site on the inositol 1,4,5-trisphosphate receptor is responsible for calmodulin inhibition, even though this inhibition requires Ca^{2+}. Mol. Pharmacol. **66**, 276–284
27 Rossi, A. and Taylor, C. W. (2004) Ca^{2+} regulation of inositol 1,4,5-trisphosphate receptors: can Ca^{2+} function without calmodulin? Mol. Pharmacol. **66**, 199–203
28 Yamaguchi, N., Xu, L., Evans, K. E., Pasek, D. A. and Meissner, G. (2004) Different regions in skeletal and cardiac muscle ryanodine receptors are involved in transducing the functional effects of calmodulin. J. Biol. Chem. **279**, 36433–36439
29 Rodney, G. G., Wilson, G. M. and Schneider, M. F. (2005) A calmodulin binding domain of RyR increases activation of spontaneous Ca^{2+} sparks in frog skeletal muscle. J. Biol. Chem. **280**, 11713–11722
30 Sencer, S., Papineni, R. V., Halling, D. B., Pate, P., Krol, J., Zhang, J. Z. and Hamilton, S. L. (2001) Coupling of RYR1 and L-type calcium channels via calmodulin binding domains. J. Biol. Chem. **276**, 38237–38241
31 Xiong, L., Zhang, J. Z., He, R. and Hamilton, S. L. (2006) A Ca^{2+}-binding domain in RyR1 that interacts with the calmodulin binding site and modulates channel activity. Biophys. J. **90**, 173–182
32 Zhu, X., Ghanta, J., Walker, J. W., Allen, P. D. and Valdivia, H. H. (2004) The calmodulin binding region of the skeletal ryanodine receptor acts as a self-modulatory domain. Cell Calcium **35**, 165–177

33 Rossi, A. M., Riley, A. M., Tovey, S. C., Rahman, T., Dellis, O., Taylor, E. J. A., Veresov, V. G., Potter, B. V. L. and Taylor, C. W. (2009) Synthetic partial agonists reveal key steps in IP_3 receptor activation. Nat. Chem. Biol. **5**, 631–639

34 Marchant, J. S. and Taylor, C. W. (1997) Cooperative activation of IP_3 receptors by sequential binding of IP_3 and Ca^{2+} safeguards against spontaneous activity. Curr. Biol. **7**, 510–518

35 Sun, Y. and Taylor, C. W. (2008) A calmodulin antagonist reveals a calmodulin-independent interdomain interaction essential for activation of inositol 1,4,5-trisphosphate receptors. Biochem. J. **416**, 243–253

36 Kasri, N. N., Török, K., Galione, A., Garnham, C., Callewaert, G., Missiaen, L., Parys, J. B. and De Smedt, H. (2006) Endogenously bound calmodulin is essential for the function of the inositol 1,4,5-trisphosphate receptor. J. Biol. Chem. **281**, 8332–8338

37 Sugawara, H., Kurosaki, M., Takata, M. and Kurosaki, T. (1997) Genetic evidence for involvement of type 1, type 2 and type 3 inositol 1,4,5-trisphosphate receptors in signal transduction through the B-cell antigen receptor. EMBO J. **16**, 3078–3088

38 Cardy, T. J. A., Traynor, D. and Taylor, C. W. (1997) Differential regulation of types 1 and 3 inositol trisphosphate receptors by cytosolic Ca^{2+}. Biochem. J. **328**, 785–793

39 Tovey, S. C., Sun, Y. and Taylor, C. W. (2006) Rapid functional assays of intracellular Ca^{2+} channels. Nat. Protoc. **1**, 259–263

40 Rahman, T. U., Skupin, A., Falcke, M. and Taylor, C. W. (2009) Clustering of IP_3 receptors by IP_3 retunes their regulation by IP_3 and Ca^{2+}. Nature **458**, 655–659

41 Bosanac, I., Yamazaki, H., Matsu-ura, T., Michikawa, M., Mikoshiba, K. and Ikura, M. (2005) Crystal structure of the ligand binding suppressor domain of type 1 inositol 1,4,5-trisphosphate receptor. Mol. Cell **17**, 193–203

42 Sienaert, I., Kasri, N. N., Vanlingen, S., Parys, J., Callewaert, G., Missiaen, L. and De Smedt, H. (2002) Localization and function of a calmodulin/apocalmodulin binding domain in the N-terminal part of the type 1 inositol 1,4,5-trisphosphate receptor. Biochem. J. **365**, 269–277

43 Ikemoto, N. and Yamamoto, T. (2002) Regulation of calcium release by interdomain interaction within ryanodine receptors. Front. Biosci. **7**, 671–683

44 Chan, J., Whitten, A. E., Jeffries, C. M., Bosanac, I., Mal, T. K., Ito, J., Porumb, H., Michikawa, T., Mikoshiba, K., Trewhella, J. and Ikura, M. (2007) Ligand-induced conformational changes via flexible linkers in the amino-terminal region of the inositol 1,4,5-trisphosphate receptor. J. Mol. Biol. **373**, 1269–1280

45 Rhoads, A. R. and Friedberg, F. (1997) Sequence motifs for calmodulin recognition. FASEB J. **11**, 331–340

46 Yoshikawa, F., Morita, M., Monkawa, T., Michikawa, T., Furuichi, T. and Mikoshiba, K. (1996) Mutational analysis of the ligand binding site of the inositol 1,4,5-trisphosphate receptor. J. Biol. Chem. **271**, 18277–18284

47 Iwai, M., Michikawa, T., Bosanac, I., Ikura, M. and Mikoshiba, K. (2007) Molecular basis of the isoform-specific ligand-binding affinity of inositol 1,4,5-trisphosphate receptors. J. Biol. Chem. **282**, 12755–12764

48 Uchida, K., Miyauchi, H., Furuichi, T., Michikawa, T. and Mikoshiba, K. (2003) Critical regions for activation gating of the inositol 1,4,5-trisphosphate receptor. J. Biol. Chem. **278**, 16551–16560

49 Ghosh, T. K., Eis, P. S., Mullaney, J. M., Ebert, C. L. and Gill, D. L. (1988) Competitive, reversible, and potent antagonism of inositol 1,4,5-trisphosphate-activated calcium release by heparin. J. Biol. Chem. **263**, 11075–11079

50 Dellis, O., Rossi, A. M., Dedos, S. G. and Taylor, C. W. (2008) Counting functional IP_3 receptors into the plasma membrane. J. Biol. Chem. **283**, 751–755

51 Yamazaki, H., Chan, J., Ikura, M., Michikawa, T. and Mikoshiba, K. (2010) Tyr-167/Trp-168 in type 1/3 inositol 1,4,5-trisphosphate receptor mediates functional coupling between ligand binding and channel opening. J. Biol. Chem. **285**, 36081–36091

52 Gangopadhyay, J. P. and Ikemoto, N. (2006) Role of the Met^{3534}–Ala^{4271} region of the ryanodine receptor in the regulation of Ca^{2+} release induced by calmodulin binding domain peptide. Biophys. J. **90**, 2015–2026

53 Adkins, C. E. and Taylor, C. W. (1999) Lateral inhibition of inositol 1,4,5-trisphosphate receptors by cytosolic Ca^{2+}. Curr. Biol. **9**, 1115–1118

54 Veresov, V. G. and Konev, S. V. (2006) Bridging the gaps in 3D structure of the inositol 1,4,5-trisphosphate-binding core. Biochem. Biophys. Res. Commun. **341**, 1277–1285

55 Bosanac, I., Alattia, J.-R., Mal, T. K., Chan, J., Talarico, S., Tong, F. K., Tong, K. I., Yoshikawa, F., Furuichi, T., Iwai, M. et al. (2002) Structure of the inositol 1,4,5-trisphosphate receptor binding core in complex with its ligand. Nature **420**, 696–700

56 Lin, C. C., Baek, K. and Lu, Z. (2011) Apo and InsP_3-bound crystal structures of the ligand-binding domain of an InsP_3 receptor. Nat. Struct. Mol. Biol. **18**, 1172–1174

Received 26 June 2012/13 September 2012; accepted 26 September 2012
Published as BJ Immediate Publication 26 September 2012, doi:10.1042/BJ20121034

Biochem. J. (2013) **449**, 39–49 (Printed in Great Britain) doi:10.1042/BJ20121034

online data

SUPPLEMENTARY ONLINE DATA

Activation of IP_3 receptors requires an endogenous 1-8-14 calmodulin-binding motif

Yi SUN[1,2], Ana M. ROSSI[1], Taufiq RAHMAN and Colin W. TAYLOR[3]

Department of Pharmacology, University of Cambridge, Cambridge CB2 1PD, U.K.

			1 8 14		
MLCK peptide			RRKWQKTGHAVRAIGRL		+6
1-8-14 consensus			1XXX5XX8XXXXX14		
rat	IP_3R1	46	LNNPPKKFRDCLFKLCPMNRYSAQKQ	71	+4
rat	IP_3R2	46	LTNPPKKFRDCLFKVCPMNRYSAQKQ	71	+4
rat	IP_3R3	45	LDNPPKKFRDCLFKVCPMNRYSAQKQ	70	+4
chicken	IP_3R1	46	LNNPPKKFRDCLFKLCPMNRYSAQKQ	71	+4
chicken	IP_3R2	48	LANPPKKFRDCLFKVCPMNRYSAQKQ	73	+4
chicken	IP_3R3	45	LDNPPKKFRDCLFKVCPMNRYSAQKQ	70	+4
frog	IP_3R1	46	LNNPPKKFRDCLFRLCPMNRYSAQKQ	71	+4
frog	IP_3R2	46	LANPPKKFRDCLFKVCPMNRYSAQKQ	71	+4
frog	IP_3R3	45	LDNPPKKFRDCLFRVCPMNRYSAQKQ	70	+4
Drosophila	IP_3R	49	LSCPPKKFRDCLIKICPMNRYSAQKQ	74	+4
C. elegans	IP_3R	124	PESPPKKFRDCLFKVCPVNRYAAQKH	149	+4
rabbit	RyR1	59	PP-DLAICCFTLEQSLSV	75	−2
rabbit	RyR2	59	PP-DLSICTFVLEQSLLV	75	−2
rabbit	RyR3	59	PP-DLCVCNFVLEQSLSV	75	−2

Figure S1 A conserved 1-8-14 motif in all IP_3Rs and RyRs

Alignments (with first and last residues numbered) of the N-terminal region of rat IP_3R1–IP_3R3 (SwissProt accession numbers NP_001007236, NP_112308 and NP_037270 respectively), chicken IP_3R1–IP_3R3 (SwissProt accession numbers XP_414438, XP_001235613 and XP_418035 respectively), *Xenopus* IP_3R1–IP_3R3 (SwissProt accession numbers NP_001084015, ABP88141 and ABP88140 respectively), *Drosophila* IP_3R (SwissProt accession number NP_730942), *Caenorhabditis elegans* IP_3R (SwissProt accession number NP_001023170) and rabbit RyR1–RyR3 (SwissProt accession numbers P11716, P30957 and Q9TS33 respectively) highlighting the residues proposed to form a 1-8-14 CaM-binding motif. The consensus sequence for a 1-8-14 motif is shown in the first row, with its three critical (1, 8 and 14 hydrophobic residues) and net charge of $+3$ to $+6$. A similar 1-8-14 motif is conserved in all IP_3R, which closely resembles a type A (1-5-8-14) motif, where position 5 is also a large hydrophobic residue. The motif within IP_3Rs differs from a classic 1-8-14 consensus sequence by having a tyrosine residue at position 14. All subtypes of RyR also have a similar 1-8-14 motif within a similar position in the three-dimensional structure, although the sequence lacks the usual net positive charge of a consensus 1-8-14 motif.

[1] These authors contributed equally to this work.
[2] Present address: Wellcome Trust Sanger Institute, Wellcome Trust Genome Campus, Hinxton, Cambridge CB10 1SA, U.K.
[3] To whom correspondence should be addressed (email cwt1000@cam.ac.uk).

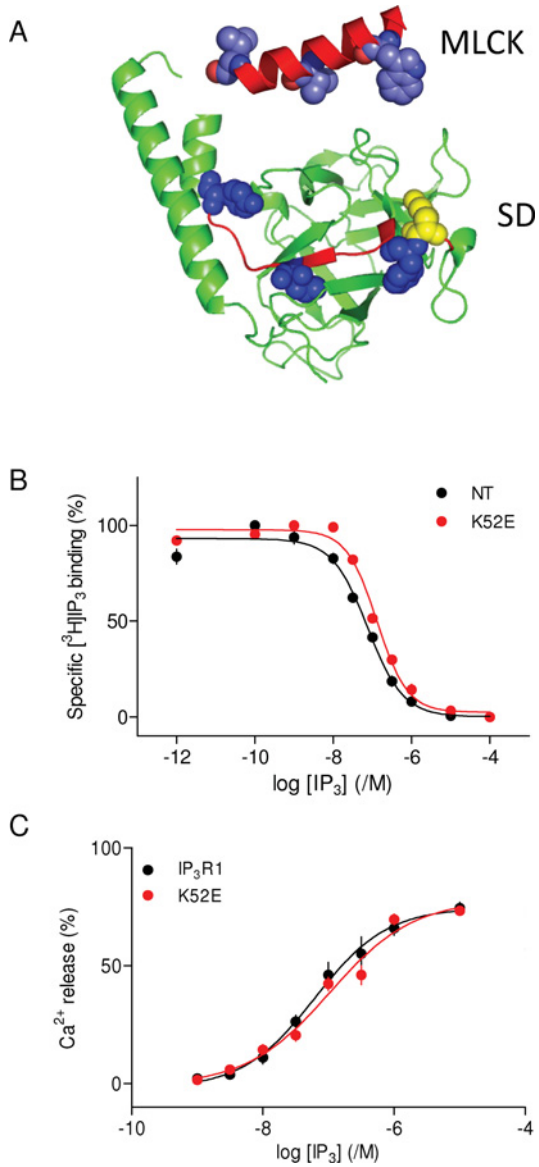

Figure S2 Mutation of a non-critical residue (K52E) within the 1-8-14 motif has no effect on IP_3 binding or IP_3-evoked Ca^{2+} release

(**A**) Structure of the SD of IP_3R1 (PDB code 1XZZ) highlighting the 1-8-14 motif (red), the critical 1-8-14 hydrophobic residues (blue) and Lys^{52} (yellow). (**B**) Equilibrium competition binding of IP_3 (with 0.75 nM [^{3}H]IP_3) to native NT and NT^{K52E}. (**C**) IP_3-evoked Ca^{2+} release from DT40-IP_3R1 and DT40-IP_3R1^{K52E} cells. Results are means $\pm$ S.E.M. ($n \geqslant 3$).

Table S1 Peptides used in the present study

All peptides were synthesised by Sigma or New England Peptide. The isolelectric point (pI) is shown for each peptide calculated from http://www.innovagen.se/custom-peptide-synthesis/peptide-property-calculator/peptide-property-calculator.asp. Ac, acetyl.

Peptide	Sequence	Source	pI
MLCK	Ac-RRKWQKTGHAVRAIGRL-NH_2	Ca^{2+}–CaM-binding site of smooth muscle MLCK	14.0
1-8-14	Ac-KKFRDALFKLAPMNRY-NH_2	Fragment of IP_3R1 (residues 51–66) containing the 1-8-14 motif	11.6
$1\text{-}8\text{-}14^C$	Ac-KK**E**RDALFKLAPMNR**E**-NH_2	Inactive form of 1-8-14 peptide (mutations highlighted in bold and underlined)	10.8
$1\text{-}8\text{-}14^S$	Ac-AMRFLKYLPKRFDKNA-NH_2	Scrambled form of 1-8-14 peptide	11.6
$1\text{-}8\text{-}14^L$	Ac-LNNPPKKFRDALFKLAPMNRYSAQKQFWKA-NH_2	Longer fragment of IP_3R1 (residues 46–75) containing the 1-8-14 motif	11.7

Table S2 Primers used in the present study

Primers used for introducing mutations in the N-terminal fragment or full-length IP_3R1. The mutated bases are highlighted.

Primer	Sequence (5′→3′)
F53E Forward	GGGGACCTTAACAATCCACCCAAGAAA**GAG**AGAGACTGCCTCTT
F53E Reverse	AAGAGGCAGTCTCT**CTC**TTTCTTGGGTGGATTGTTAAGGTCCCC
L60E Forward	GAAATTCAGAGACTGCCTCTTTAAG**GAG**TGTCCTATGAATCGATATTCTGCA
L60E Reverse	TGCAGAATATCGATTCATAGGACA**CTC**CTTAAAGAGGCAGTCTCTGAATTTC
Y66E Forward	CTCTTTAAGCTATGTCCTATGAATCGA**GAG**TCTGCACAGAAGCAG
Y66E Reverse	CTGCTTCTGTGCAGA**CTC**TCGATTCATAGGACATAGCTTAAAGAG
K52E Forward	AACAATCCACCCAAG**GAA**TTCAGAGACTGCCTC
K52E Reverse	GAGGCAGTCTCTGAA**TTC**CTTGGGTGGATTGTT

Received 26 June 2012/13 September 2012; accepted 26 September 2012
Published as BJ Immediate Publication 26 September 2012, doi:10.1042/BJ20121034